Eur. Phys. J. B **36**, 161–167 (2003)
DOI: 10.1140/epjb/e2003-00330-1

THE EUROPEAN PHYSICAL JOURNAL B

Electronic state anisotropy and the Fermi surface topology of the incommensurate organic superconducting crystal (MDT-TSF)(AuI_2)$_{0.436}$

T. Kawamoto[1,a], T. Mori[1], C. Terakura[2], T. Terashima[2], S. Uji[2], H. Tajima[3], K. Takimiya[4], Y. Aso[4], and T. Otsubo[4]

[1] Department of Organic and Polymeric Materials, Graduate School of Science and Engineering, Tokyo Institute of Technology, O-okayama, Meguro-ku, Tokyo 152-8552, Japan
[2] National Institute for Materials Science, Tsukuba, Ibaraki 305-0003, Japan
[3] Institute for Solid State Physics, The University of Tokyo, Kashiwanoha, Kashiwa-shi, Chiba 277-8581, Japan
[4] Department of Applied Chemistry, Graduate School of Engineering, Hiroshima University, Kagamiyama, Higashi-Hiroshima, Hiroshima 739-8527, Japan

Received 15 August 2003
Published online 8 December 2003 –

Abstract. The Fermi surface (FS) shape of the organic superconductor (MDT-TSF)(AuI_2)$_{0.436}$ with an incommensurate anion structure (MDT-TSF: methylenedithio-tetraselenafulvalene) has been investigated by means of the optical reflectance spectra and angular-dependent magnetoresistance oscillations (AMRO). The difference of the plasma frequencies between the interstack and the intrastack directions indicates that the overall band structure has small anisotropy ($\omega_{p,\perp}/\omega_{p,\parallel} \approx 0.62$). The observation of the AMRO shows the presence of a small closed orbit, which can be assigned to the overlapped area of the large FS. This demonstrates that the incommensurate anion potential is crucial to remove the degeneracy of the energy bands on the zone boundary. The magnetoresistance peak in the fields applied within the conducting layers shows an unusually large interlayer transfer integral ($t_\perp \approx 1$ meV) among organic superconductors.

PACS. 74.70.Kn Organic superconductors – 71.18.+y Fermi surface

1 Introduction

Recently, Takimiya et al. have synthesized MDT-TSF (Fig. 1a), and have discovered superconductivity (T_c = 4.5 K) in the AuI_2 salt [1]. Although most organic superconductors form commensurate crystals [2,3], the anion lattice of this compound is incommensurate to the donor lattice, and the resulting composition is non-stoichiometric, and is represented as (MDT-TSF)(AuI_2)$_{0.436}$ [4]. As shown in Figure 1b, this salt has a uniform donor stacking along the a-axis and the donors form a conducting sheet on the ab plane.

A superconductor with an incommensurate periodic potential is a unique material. Azbel has theoretically pointed out that a clean metal with an incommensurate periodic potential shows a fine structure of quantum oscillations associated with the multiply folded first Brillouin zone (BZ) [5]. Recently, we have performed the Shubnikov-de Haas (SdH) oscillation measurements to verify this prediction [6]. We have not, however, observed such many different frequencies coming from the multiple folding, but found several frequencies all of which are assigned to the orbits of the original FS's and the reconstructed ones obtained from a single shift of the BZ by $3\boldsymbol{q}$, where $\boldsymbol{q}$ is the fundamental wave vector of the anion lattice. This may be related to the fact that the $3\boldsymbol{q}$ spots in the X-ray superlattice reflection are very strong. The FS reconstruction occurs only by a single shift associated with the most dominant superlattice potential.

Although the FS reconstruction due to the incommensurate anion potential is proved by the SdH oscillation experiments, we have to assume a relatively small transverse interaction to explain the observed SdH oscillations [6]. Thus precise estimation of the FS anisotropy is indispensable. In addition, the SdH oscillation originating in the small orbit (γ-orbit) appears from lower magnetic fields than the magnetic breakdown orbit of the large FS (δ-orbit) is observed (Fig. 1c); this indicates that the degeneracy of the zone boundary, which is intrinsic to the donor lattice, is removed by the incommensurate anion potential. A similar effect coming from the incommensurate anion potential is expected in other methods to investigate the FS shape. In the present paper, two kinds of experiments

[a] e-mail: kawamoto@o.cc.titech.ac.jp

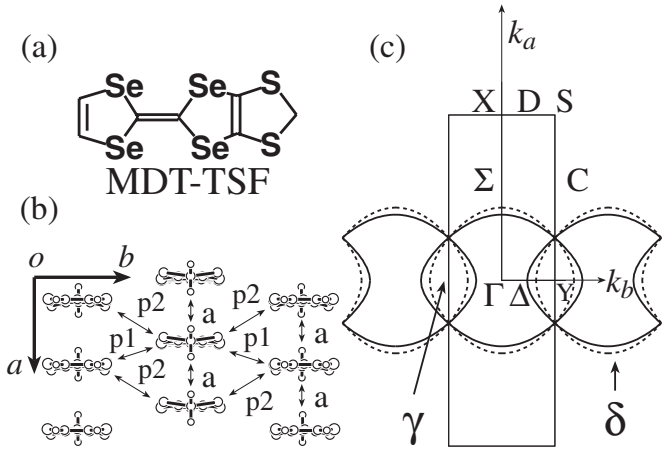

Fig. 1. (a) MDT-TSF molecule, (b) donor arrangement projected along the molecular long axis, and (c) the Fermi surface calculated on the basis of the extended Hückel method from the donor lattice. The dotted Fermi surface is calculated based on the transfer integrals ($t_{\rm a} = 272.7$, $t_{\rm p1} = -30.6$, and $t_{\rm p2} = -128.2$ meV) obtained from the atomic parameter set (I), and the solid curve is the result by the transfer integrals ($t_{\rm a} = 106.9$, $t_{\rm p1} = -10.3$, and $t_{\rm p2} = -35.4$ meV) estimated from the parameter set (II).

have been carried out to determine the FS shape and anisotropy.

First, the polarized optical reflectance has been measured to obtain the original FS (δ-orbit) without the effect of the incommensurate lattice. Previously, the electronic state anisotropy of many organic conductors has been investigated by the optical experiments [7–13]. The overall band structure is explored by the combination of the plasma frequencies obtained from the analysis of the optical measurements and the tight-binding calculations.

Second, the angular dependent magnetoresistance oscillations (AMRO) have been measured to clarify the detail of the FS topology. Although magnetic quantum oscillations do not provide any details of the shape of the FS sections, the AMRO gives accurate information about the shape of the FS [14,15]. The influence of the incommensurate anion potential is investigated by the analysis of the AMRO.

2 Experiment

Single crystals were prepared by the electrocrystallization [1].

The optical reflectance spectra were measured by the use of Olympus MMSP micro spectrophotometer from 4200 cm^{-1} to 25000 cm^{-1} and with an FT-IR micro spectrophotometer (Jasco FT/IR-620) from 650 cm^{-1} to 7000 cm^{-1} at room temperature.

The energy band structure was calculated based on the extended Hückel method and the tight-binding approximation. The band calculation is another good method to estimate the anisotropy, but the resulting anisotropy is sometimes sensitive to the adopted parameters (Fig. 1c). For comparison, we examined two kinds of atomic orbital parameters: set (I) with Se 4d and S 3d orbitals, and set (II) without these orbitals [16,17]. The transfer integrals, t_i, are estimated from the intermolecular overlap integrals S_i as $t_i = E \times S_i$, in which the energy level of the highest occupied molecular orbital (HOMO) E is taken to be -10 eV. The interaction modes (a, p1, and p2) are defined in Figure 1b.

For the AMRO measurements, the samples were mounted on a cryostat in a 14 T superconducting magnet with two degrees of rotational freedom with respect to the magnetic field, and was cooled to 1.7 K. To improve the signal to noise ratio, relatively large ac current (about 1 mA) was applied along the c-axis. No appreciable heating effect due to the current was found. Lock-in and preamplifiers were used for the high-sensitive detection.

3 Results and discussion

3.1 Optical reflectance

Figure 2a shows optical reflectance spectra for two polarization axes ($\parallel a$ and $\parallel b$) at room temperature. Both spectra show clear plasma edges even at room temperature, in contrast to the relatively obscure plasma edges observed in some ET salts like κ-(ET)$_2$Cu(NCS)$_2$ [ET: bis(ethylenedithio)tetrathiafulvalene] [18–20]. The $\parallel a$ dispersion is much larger than that along b, supporting the relatively small transverse ($\parallel b$) interaction assumed in the SdH measurements. More careful analysis is, however, necessary for quantitative estimation.

The spectrum along the a axis shows the Drude response with a broad peak around 3000 cm^{-1}. Therefore, the $\parallel a$ spectrum can be analyzed by the Drude-Lorentz model described by the following equations [7,13,21]:

$$R = \left| \frac{\sqrt{\tilde{\epsilon}} - 1}{\sqrt{\tilde{\epsilon}} + 1} \right|^2, \tag{1}$$

$$\tilde{\epsilon} = \epsilon_\infty - \frac{\omega_p^2}{\omega^2 + i\omega\Gamma} - \sum_j \frac{\omega_{pj}^2}{(\omega^2 - \omega_j^2) + i\omega\Gamma_j}, \tag{2}$$

where R is the reflectance, $\tilde{\epsilon}$ is the complex dielectric function, ϵ_∞ stands for the frequency-independent dielectric constant, ω_p and Γ are the plasma frequency and the relaxation rate of the charge carriers, and ω_j, Γ_j, ω_{pj} are the parameters of the Lorentz oscillators for simulating the other dispersions. The obtained Drude-Lorentz parameters are $\epsilon_{\infty,a} = 3.85$, $\Gamma_a = 0.11$ eV, $\omega_{p,a} = 0.88$ eV, $\omega_1 = 0.27$ eV, $\Gamma_1 = 0.28$ eV, and $\omega_{p1} = 0.82$ eV, respectively. The conductivity spectrum has been calculated as

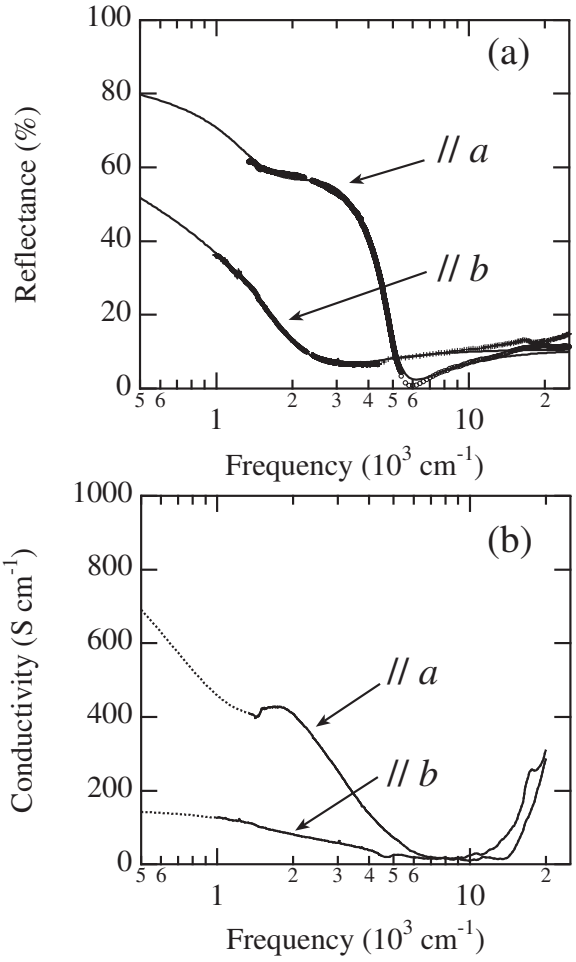

Fig. 2. (a) Optical reflectance spectra and (b) optical conductivities at room temperature. The solid lines in the upper figure is the Drude-Lorentz fit. The solid lines in the lower figure represent experimental results and the dotted lines show the extrapolation.

shown in Figure 2b by the Kramers-Kronig transformation based on the extrapolated reflectance, $R(\omega)$, on the assumption of the Drude-Lorentz model in the low frequency region.

The $\parallel b$ spectrum shows the simple Drude response. This spectrum has been analyzed by the simple Drude model without Lorentz oscillator in the above equation. The obtained Drude parameters are $\epsilon_{\infty,b} = 3.88$, $\Gamma_b = 0.27$ eV, and $\omega_{p,b} = 0.55$ eV, respectively. The conductivity spectrum has been calculated as shown in Figure 2b by the same method as the $\parallel a$ spectrum.

From the plasma frequency, we can estimate the effective mass by using $m^* = n\,e^2/(\epsilon_0\,\omega_p^2)$, where n is the hole number density. The effective mass is estimated to be $2.4m_0$ and $6.1m_0$ for $\parallel a$ and $\parallel b$ (m_0 is the free electron mass), respectively. The averaged effective mass, $\langle m^*_{\rm opt}\rangle = \sqrt{m^*_{a,\rm opt} m^*_{b,\rm opt}} = 3.8m_0$, is almost in agreement with the averaged δ-orbit effective cyclotron mass ($\langle m^*_{c,\delta}\rangle = \sqrt{m^*_{\delta_1} m^*_{\delta_2}} = 4.3m_0$) evaluated from the SdH result. The effective cyclotron mass is only slightly larger than the optical mass by 10%. In some ET superconductors, the cyclotron mass is typically 1.2–1.7 times larger than the optical mass [11,18–20,22–30]. The small difference in the present compound may suggest the relative unimportance of the many-body effect.

The optical zero-frequency conductivity along the a axis, $\sigma_{\rm opt}(0)$, is estimated as $\sigma_{\rm opt}(0) = \epsilon_0\omega_p^2/\Gamma = 960$ S cm^{-1}, which is in good agreement with the dc conductivity $\sigma_{\rm dc} \approx 1000$ S cm^{-1} from our transport measurements.

The Fermi energy is represented by $E_F = \hbar^2\,k_{F,\alpha}^2/(2m_\alpha^*)$ upon the assumption of a parabolic energy band, where $k_{F,\alpha}$ is the Fermi wave number along the α-direction. Therefore, through the anisotropy of the effective mass, the principal Fermi wave number, $k_{F,\alpha}$, is related to the corresponding plasma frequency, $\omega_{p,\alpha}$, as $k_{F,\alpha} \propto 1/\omega_{p,\alpha}$. From the ratio of the principal plasma frequencies, we can estimate the anisotropy of the Fermi wave number as $k_{F,a}/k_{F,b} = \omega_{p,b}/\omega_{p,a} = 0.62$, assuming an elliptical FS. This indicates small anisotropy in the ab plane. This elliptical δ-orbit makes the γ-orbit cross sectional area 12.4% of the first BZ. This γ-orbit area is a little larger than that obtained from the SdH results (10.4%). This is because the above estimation does not include the influence of the energy gap at the zone boundary. Therefore, the obtained Fermi wave number ratio (0.62) may be smaller than our previous estimation from the SdH frequencies of the γ-orbit (0.75) [6]. The band calculation based on the atomic orbital parameter set (I) gives too isotropic result ($k_{F,a}/k_{F,b} = 0.93$) (Fig. 1c). If we use the parameter set (II), the anisotropy is enhanced ($k_{F,a}/k_{F,b} = 0.72$), and reproduces the estimation from the optical and the SdH experiments.

The $\parallel a$ conductivity spectrum has a shoulder around 1700 cm^{-1} (Fig. 2b), which is reproduced by a Lorentz oscillator in the reflectance spectrum. This may be attributed to the interband transition in analogy with β-$(ET)_2I_3$ [9]. We can explain the broad peak from the interband transition according to the band calculation. The α-direction plasma frequency is calculated by the following equation derived from the Boltzmann equation [7,10,21],

$$\omega_{p,\alpha}^2 = \frac{ne^2}{\epsilon_0\hbar^2}\frac{\iiint \frac{\partial^2 E(k)}{\partial k_\alpha^2} f(E(k))dk_a dk_b dk_c}{\iiint f(E(k))dk_a dk_b dk_c} \qquad (3)$$

where $E(k)$ is the energy dispersion and $f(E(k))$ is the Fermi-Dirac distribution function. We have divided the first BZ into 40×40 meshes, and numerically integrated the second derivatives of $E(k)$ at $T = 0$ K. The calculated $\omega_{p,a}$ and $\omega_{p,b}$ are 0.85 eV and 0.61 eV, respectively, under the parameter set (II). These values are in good agreement with the experimental estimation (0.88 eV and 0.55 eV). From the theoretically evaluated plasma frequencies, the averaged effective mass is calculated as

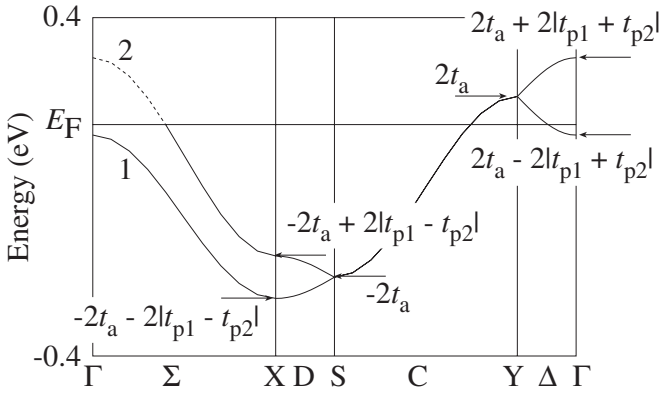

Fig. 3. Energy band structure. The dotted line (band 2) shows the region where the interband transition from the band 1 to the band 2 is possible.

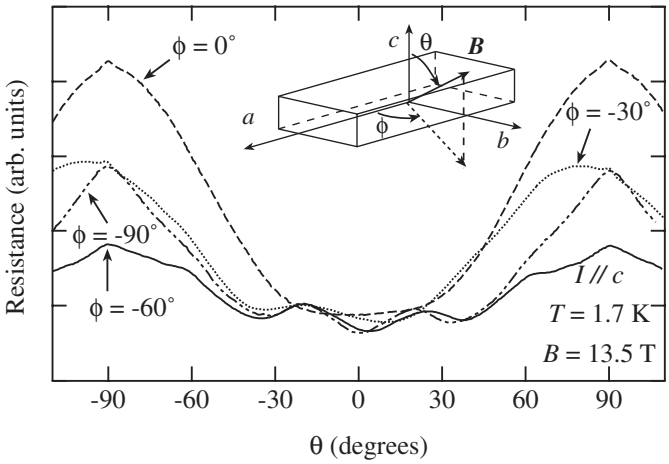

Fig. 4. Angular-dependent magnetoresistance oscillations (AMRO) at 1.7 K for $B = 13.5$ T.

$\langle m^*_{\rm calc}\rangle = \sqrt{m^*_{a,\rm calc} m^*_{b,\rm calc}} = 3.6m_0$, where $m^*_{a,\rm calc} = 2.6m_0$ and $m^*_{b,\rm calc} = 5.1m_0$, in agreement with the value of the averaged δ-orbit ($4.3m_0$) in the SdH result.

The interband transition can be explained from the tight-binding energy band

$$E(k_a, k_b) = \pm 2\sqrt{(t_{\rm p1} + t_{\rm p2})^2 - 4t_{\rm p1}t_{\rm p2}\sin^2(k_a a/2)} \times \cos(k_b b/2) + 2t_a \cos(k_a a). \quad (4)$$

Figure 3 shows the energy band structure calculated by using the parameter set (II). Although the obtained energy band splits on the Σ line owing to $t_{\rm p1} \neq t_{\rm p2}$, the energy band is degenerated on the C line on account of the lattice symmetry ($Pnma$). Therefore, the interband transition occurs from the band 1 to the band 2 on the Σ line. This is consistent with the presence of the shoulder in the $\parallel a$ conductivity spectrum. Contrarily, the interband transition is absent along the b-axis. The band splitting at the Γ point is $4|t_{\rm p1} + t_{\rm p2}| = 183$ meV~ 1500 cm^{-1}, which is close to the shoulder ($\omega_0 \sim 1700$ cm$^{-1} \sim 210$ meV) of the $\parallel a$ conductivity spectrum.

In summary, the optical spectra lead to the in-plane anisotropy to be $\sqrt{m^*_{a,\rm opt}/m^*_{b,\rm opt}} \sim k_{F,a}/k_{F,b} \sim 0.62$. The $\parallel a$ spectrum indicates that the interband gap is about 210 meV.

3.2 Magnetoresistance

Figure 4 shows angle dependence of the magnetoresistance for $I \parallel c$ at 1.7 K under the field of 13.5 T. The angles θ and ϕ are defined in the inset. According to Yamaji's theory [31], the magnetoresistance peaks for the simple corrugated cylindrical FS appear with the $\tan\theta$ periodicity,

$$\Delta \tan\theta = \frac{\pi}{k_\parallel(\phi) d_\perp} \quad (5)$$

and the projection wave number $k_\parallel(\phi)$ is

$$k_\parallel(\phi) = \sqrt{k^2_{F,\rm max}\cos^2(\phi - \xi) + k^2_{F,\rm min}\sin^2(\phi - \xi)} \quad (6)$$

for an elliptical FS [15,32]. Here $d_\perp$ is the effective interlayer spacing ($d_\perp = c/2 = 12.712$ Å), $k_{F,\rm min}$ ($k_{F,\rm max}$) is the minimum (maximum) Fermi wave number, and ξ is the inclination of the principal axis from the a-axis.

Figure 5a shows the resistance and the second derivative ($-d^2R/d\theta^2$) as a function of $\tan\theta$ for $\phi = -60°$. We have measured the resistance down to 8 T and found that the characteristic peak features in the second derivative are independent of the magnetic field. Therefore, the peaks are not associated with the quantum oscillation, but come from the AMRO. In our previous paper [6], we have reported several SdH oscillations observed in a wide field range up to 18 T, which indicate the presence of coherent cyclotron motion along the closed orbits. The main SdH oscillation i.e. the main electron trajectory is assigned to the two-dimensional FS formed around the Y point (γ-orbit) in the original BZ (Fig. 1c). Therefore, it is quite likely that the AMRO shown in Figure 4 arises from the same two-dimensional FS.

The AMRO peaks can be well defined in $-d^2R/d\theta^2$ curves in Figure 5a. We see that the period of the AMRO, $\Delta\tan\theta$, is ~ 1.8 at $\phi = -60°$. Figure 5b shows a polar plot of $k_\parallel(\phi)$ determined by equation (5). The solid line is the fitting result according to equation (6) with $k_{F,\rm min} = 0.126$ Å^{-1}, $k_{F,\rm max} = 0.187$ Å^{-1}, and $\xi = 88°$. The deviation from 90° is regarded as the setting error of the sample. The shaded area corresponds to the cross section of the FS. The cross sectional-area of this FS, 7.4×10^{-2} Å^{-2} (9.4% of the first BZ), is in good agreement both with the γ-orbit observed in the SdH measurements (10.4% of the first BZ) and with the band calculation based on the parameter set (II) (8.5% of the first BZ) [6].

The present AMRO detects the γ-orbit (Fig. 1c). This situation is the same as that of κ-$(ET)_2Cu(NCS)_2$ with

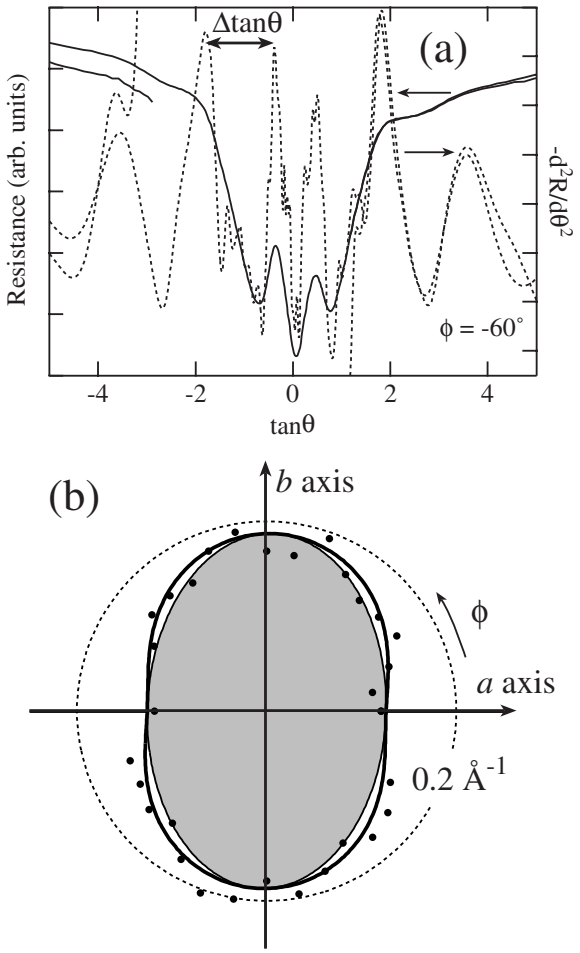

Fig. 5. (a) Resistance (solid line) and the second derivative (dotted line) as a function of $\tan\theta$ for $\phi = -60°$. (b) Polar plot of $k_{\parallel}(\phi)$. The solid line is the fitting result. The shaded area corresponds to the cross section of the FS.

a gap along the zone boundary [33], in which the magnetic break down has been observed under high magnetic field [29,30]. On the other hand, κ-$(ET)_2I_3$, which has the degenerated energy band along the zone boundary, shows the quantum oscillation originating in the large orbital from the low magnetic field [26–28]. The AMRO of this compound detects the large circular FS [28]. This difference is explained by the difference of their space groups, $P2_1$ for the $Cu(NCS)_2$ salt and $P2_1/c$ for the I_3 salt [34]. The degeneracy of the energy bands on the zone boundary occurs when the crystal has glide planes or screw axes having translation perpendicular to the boundary [35]. The donor lattice of the present compound has a twofold screw axis along the b axis (space group $Pnma$), so that the band structure is degenerated on the C zone boundary (Fig. 3). This should lead to the observation of the δ-orbit. The actual detection of the γ-orbit both in the previous SdH investigation and in the present AMRO measurement indicates that the incommensurate anion potential destroys the screw symmetry, generating a small energy gap on the C line.

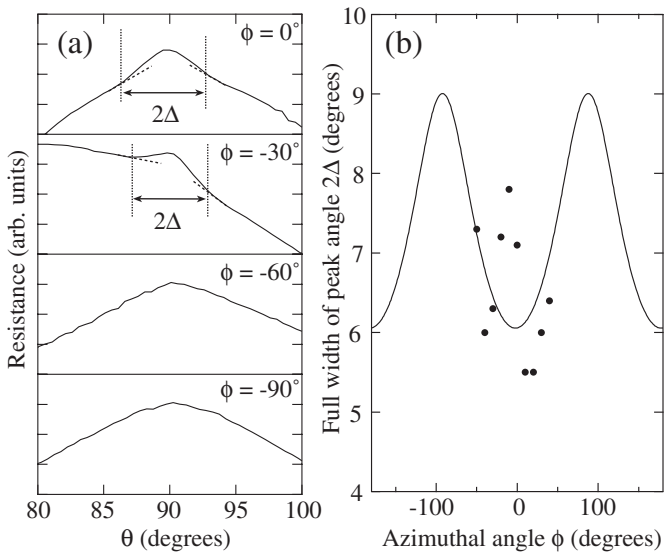

Fig. 6. (a) Peak structure of the AMRO under the magnetic fields for various azimuthal angles ϕ. (b) Angular width 2Δ of peak versus azimuthal angle ϕ. Points are the observed 2Δ and the curve represents the prediction from equation (7) with $t_\perp = 1.06$ meV.

The magnetoresistance for the magnetic fields nearly parallel to the conducting plane has a peak structure as shown in Figure 6a. This structure is ascribed to the closed orbits formed on the side of the corrugated two-dimensional FS. The peak structure indicates that the present compound has a coherent interlayer transport [36,37]. Hanasaki et al. have estimated the interlayer transfer integral, $t_\perp$, of β-$(ET)_2I_3$ from the peak width, 2Δ, by using $2\Delta = (4t_\perp d_\perp m^*)/(\hbar^2 k_F)$ [36]. Singleton et al. have analyzed the peak effect of κ-$(ET)_2Cu(NCS)_2$ by including the azimuthal angle dependence [38]. For the corrugated cylindrical ellipsoid FS, the peak effect is written by

$$2\Delta(\phi) = \frac{4t_\perp d_\perp m^*(\phi)}{\hbar^2 k_F(\phi)} = \frac{4t_\perp d_\perp m^*}{\hbar^2\sqrt{k_{F,\max}^2 \sin^2(\phi-\xi) + k_{F,\min}^2 \cos^2(\phi-\xi)}}. \quad (7)$$

Here, we use the characteristic Fermi wave numbers estimated from the AMRO analysis and the effective mass, $m^* = 2.8m_0$, of the γ-orbit determined by the SdH oscillations [6]. The observed peak widths 2Δ are plotted as a function of the azimuthal angle ϕ in Figure 6b. The fitting curve in Figure 6b gives $t_\perp = 1.06$ meV. This is much larger than $\hbar/\tau \approx 0.16$ meV estimated from the Dingle temperature of the γ-orbit of about 0.3 K corresponding to the scattering time $\tau \approx 4.1$ ps [6]. The large $t_\perp$, satisfying the condition $\hbar/\tau \ll t_\perp$, again indicates the coherent interlayer interaction.

The estimated interlayer transfer integral, $t_\perp \approx 1$ meV, is much larger than those in other organic conductors; the reported $t_\perp$ is 0.04 meV for κ-$(ET)_2Cu(NCS)_2$ [38], 0.06 meV for κ-$(ET)_2I_3$ [39], and 0.5 meV for β-$(ET)_2I_3$ [22]. The obtained value is, however, in agreement with the value estimated from the splitting of the SdH oscillations ($t_\perp \sim 2$ meV) [6]. This also agrees with the long interlayer Ginzburg-Landau coherence length ($\xi_c(0) \approx 50$ Å) [4]. The present compound has a quasi-two-dimensional electronic system with a relatively large interlayer interaction. Although most of the two-dimensional organic conductors have flat donor sheets well separated by the anions, the anions of the present compound do not make a well-defined layer, but the donors have direct inter-layer contacts [1]. There are considerable inter-layer donor-donor interactions along the c-axis. This is the reason of the large three-dimensionality of the present compound.

The magnetoresistance peak, 2Δ, is not clearly observed around the b direction ($|\phi| \geq 60°$) as shown in Figure 6a. In κ-$(ET)_2Cu(NCS)_2$, the magnetoresistance peaks have been observed in all azimuthal angles. To observe the peak effect, the scattering energy, $\Delta E \sim \hbar/\tau$, should be much smaller than the energy separation $\hbar\Omega$ i.e. $\Omega\tau \gg 1$, where Ω is the cyclotron frequency. The critical field, which is given by $\Omega\tau = 1$, is written by [37]

$$B_c(\phi) = \frac{\hbar}{ed_\perp\tau}\sqrt{\frac{m^*(\phi)}{2t_\perp}}$$

$$= \sqrt{\frac{k_{F,\max}\,k_{F,\min}\,m^*}{2t_\perp[k_{F,\max}^2\sin^2(\phi-\xi)+k_{F,\min}^2\cos^2(\phi-\xi)]}} \times \frac{\hbar}{ed_\perp\tau}. \quad (8)$$

This gives the minimum and the maximum critical fields respectively as $B_{c,\min} \sim 9.1$ T for $\phi \sim 0°$ and $B_{c,\max} \sim 13.5$ T for $\phi \sim 90°$. Our magnetic field, 13.5 T, is not large enough to observe the peak effect around $\phi \sim 90°$. The large B_c is expected to reduce the peak intensity. In addition, the disappearance of the resistance peak is associated with the broad peak width, 2Δ (Fig. 6b), which in equation (7) comes from the large $t_\perp$ as well as from the large $m^*(\phi)/k_F(\phi)$ around $\phi \sim 90°$.

4 Conclusion

In summary, we determined the Fermi wave number ratio $k_{F,a}/k_{F,b} \sim 0.62$ from the optical experiments, and show the overall band structure. The AMRO shows an elliptical FS coming from the γ-orbit. This indicates that the incommensurate anion potential is important in removing the degeneracy of the energy bands on the zone boundary, in agreement with the SdH measurement. The peak effect shows a considerably large interlayer transfer integral $t_\perp \approx 1$ meV and $t_\parallel/t_\perp \sim 100$. The present compound is an anisotropic quasi-two-dimensional organic superconductor with a relatively large interlayer interaction in contrast to the usual highly two-dimensional organic superconductors with a very small interlayer interaction.

This work was partially supported by a Grant in Aid for Scientific Research (No. 14740377) from the Ministry of Education, Science, Sports and Culture. Part of this work was performed using facilities in the Spectroscopy Laboratory, the Material Design and Characterization Laboratory, ISSP.

References

1. K. Takimiya, Y. Kataoka, Y. Aso, T. Otsubo, H. Fukuoka, S. Yamanaka, Angew. Chem. Int. Ed. **40**, 1122 (2001)
2. T. Ishiguro, K. Yamaji, G. Saito, *Organic Superconductors,* 2nd edn. (Springer, Berlin, 1998)
3. J.M. Williams, J.R. Ferraro, R.J. Thorn, K.D. Carlson, U. Geiser, H.H. Wang, A.M. Kini, M.-H. Whangbo, *Organic Superconductors (Including Fullerenes)* (Prentice Hall, Englewood Cliffs, NJ, 1992)
4. T. Kawamoto, T. Mori, K. Takimiya, Y. Kataoka, Y. Aso, T. Otsubo Phys. Rev. B **65**, 140508(R) (2002)
5. M.Ya. Azbel, Phys. Rev. Lett. **43**, 1954 (1979); Zh. Eksp. Teor. Fiz. **46**, 929 (1964) [Sov. Phys. JETP **19**, 634 (1964)]
6. T. Kawamoto, T. Mori, C. Terakura, T. Terashima, S. Uji, K. Takimiya, Y. Aso, T. Otsubo, Phys. Rev. B **67**, 020508(R) (2003)
7. C.S. Jacobsen, in *Semiconductors and Semimetals,* Vol. 27 edited by E. Conwell (Academic, Tokyo, 1988), Chap. 5
8. K. Yakushi, Bull. Chem. Soc. Jpn **73**, 2643 (2000)
9. H. Tajima, K. Yakushi, H. Kuroda, G. Saito, Solid State Commun. **56**, 159 (1985)
10. H. Tajima, K. Yakushi, H. Kuroda, G. Saito, Solid State Commun. **56**, 251 (1985)
11. M. Tamura, K. Yakushi, H. Kuroda, A. Kobayashi, R. Kato, H. Kobayashi, J. Phys. Soc. Jpn **57**, 3239 (1988)
12. M. Tamura, H. Tajima, K. Yakushi, H. Kuroda, A. Kobayashi, R. Kato, H. Kobayashi, J. Phys. Soc. Jpn **60**, 3861 (1991)
13. M. Dressel, G. Grüner, *Optical Properties of Electrons in Matter* (Cambridge University Press, Cambridge, 2002)
14. J. Wosnitza, *Fermi Surfaces of Low Dimensional Organic Metals and Superconductors* (Springer, Berlin, 1996)
15. J. Singleton, Rep. Prog. Phys. **63**, 1111 (2000); J. Singleton, C. Mielke, Contemporary Phys. **43**, 63 (2002)
16. T. Mori, A. Kobayashi, Y. Sasaki, H. Kobayashi, G. Saito, H. Inokuchi, Bull. Chem. Soc. Jpn **57**, 627 (1984)
17. T. Mori, M. Katsuhara, J. Phys. Soc. Jpn **71**, 826 (2002)
18. A. Ugawa, G. Ojima, K. Yakushi, H. Kuroda, Phys. Rev. B **38**, 5122 (1988)
19. T. Sugano, H. Hayashi, M. Kinoshita, K. Nishikida, Phys. Rev. B **39**, 11387 (1989)
20. A.-K. Klehe, R.D. McDonald, A.F. Goncharov, V.V. Struzhkin, H-K. Mao, R.J. Hemley, T. Sasaki, W. Hayes, J. Singleton, J. Phys.: Condens. Matter **12**, L247 (2000)
21. F. Wooten, *Optical Properties of Solids* (Academic, New York, 1972)

22. W. Kang, G. Montambaux, J.R. Cooper, D. Jérome, P. Batail, C. Lenoir, Phys. Rev. Lett. **62**, 2559 (1989)
23. H. Tajima, H. Kanbara, K. Yakushi, H. Kuroda, G. Saito, Solid State Commun. **57**, 911 (1986)
24. M. Tamura, H. Kuroda, S. Uji, H. Aoki, M. Tokumoto, A.G. Swanson, J.S. Brooks, C.C. Agosta, T. Hannahs, J. Phys. Soc. Jpn **63**, 615 (1994)
25. T. Terashima, S. Uji, H. Aoki, M. Tamura, M. Kinoshita, M. Tokumoto, Solid State Commun. **91**, 595 (1994)
26. K. Oshima, H. Yamazaki, K. Kato, Y. Maruyama, R. Kato, A. Kobayashi, H. Kobayashi, Synth. Met. **55-57**, 2334 (1993)
27. M. Heinecke, K. Winzer, D. Schweitzer, Z. Phys. B **93**, 45 (1993)
28. P. Helm, W. Kraak, D. Schweitzer, H.J. Keller, Phys. Status Solidi (b) **189**, 509 (1995)
29. T. Sasaki, H. Sato, N. Toyota, Solid State Commun. **76**, 507 (1990)
30. J. Caulfield, W. Lubczynski, F.L. Pratt, J. Singleton, D.Y.K. Ko, W. Hayes, M. Kurmoo, P. Day, J. Phys.: Condens. Matter **6**, 2911 (1994)
31. K. Yamaji, J. Phys. Soc. Jpn **58**, 1520 (1989)
32. A.A. House, N. Harrison, S.J. Blundell, I. Deckers, J. Singleton, F. Herlach, W. Hayes, J.A.A.J. Perenboom, M. Kurmoo, P. Day, Phys. Rev. B **53**, 9127 (1996)
33. M.-S. Nam, M.M. Honold, C. Proust, N. Harrison, C.H. Mielke, S.J. Blundell, J. Singleton, W. Hayes, M. Kurmoo, P. Day, Synth. Met. **103**, 1905 (1999)
34. K. Oshima, T. Mori, H. Inokuchi, H. Urayama, H. Yamochi, G. Saito, Phys. Rev. B **38**, 938 (1988)
35. G. Burns, *Introduction to Group Theory with Applications* (Academic, New York, 1977)
36. N. Hanasaki, S. Kagoshima, T. Hasegawa, T. Osada, N. Miura, Phys. Rev. B **57**, 1336 (1998)
37. R.H. McKenzie, P. Moses, Phys. Rev. Lett. **81**, 4492 (1998); P. Moses, R.H. McKenzie, Phys. Rev. B **60**, 7998 (1999)
38. J. Singleton, P.A. Goddard, A. Ardavan, N. Harrison, S.J. Blundell, J.A. Schlueter, A.M. Kini, Phys. Rev. Lett. **88**, 037001 (2002)
39. J. Wosnitza, J. Hagel, J.S. Qualls, J.S. Brooks, E. Balthes, D. Schweitzer, J.A. Schlueter, U. Geiser, J. Mohtasham, R.W. Winter, G.L. Gard, Phys. Rev. B **65**, 180506(R) (2002)